Materials & Design 207 (2021) 109839

Contents lists available at ScienceDirect

Materials & Design

journal homepage: www.elsevier.com/locate/matdes

Self-healing behavior of epoxy-based double-layer nanocomposite coatings modified with Zirconia nanoparticles

Sehrish Habib [a,c], Amani Hassanein [a], Ramazan Kahraman [b,*], Elsadig Mahdi Ahmed [c], R.A. Shakoor [a,*]

[a] Center for Advanced Materials (CAM), Qatar University, 2713 Doha, Qatar
[b] Department of Chemical Engineering, Qatar University, 2713 Doha, Qatar
[c] Department of Mechanical and Industrial Engineering, Qatar University, 2713 Doha, Qatar

HIGHLIGHTS

- Self-healing performance of epoxy-based double-layer coatings are reported.
- The epoxy matrix is reinforced with modified zirconia (ZrO_2) nanoparticles.
- ZrO_2 nanoparticles are modified with Imidazole and PEI as the self-healing agent.
- Epoxy-based nanocomposite coatings are deposited as pre and topcoat on substrate.
- EIS results demonstrated good corrosion resistance of double-layer coatings.

GRAPHICAL ABSTRACT

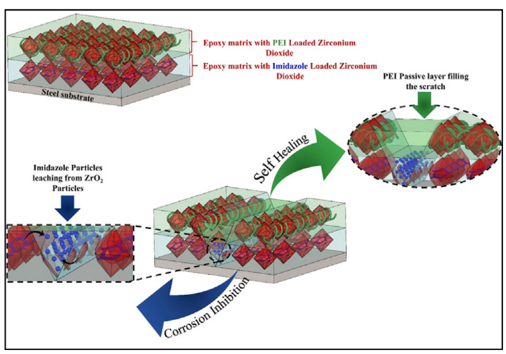

ARTICLE INFO

Article history:
Received 14 March 2021
Revised 2 May 2021
Accepted 17 May 2021
Available online 18 May 2021

Keywords:
Zirconia nanoparticles
Epoxy
Double layer
Nanocomposite coatings
Corrosion behavior

ABSTRACT

This work reports the self-healing behavior of epoxy-based double-layer nanocomposite coatings designed to mitigate corrosion in various industrial applications. Zirconia (ZrO_2) nanoparticles were used as a carrier to load separately self-healing agent, polyethyleneimine (PEI), and corrosion inhibitor, imidazole (IM). The loaded ZrO_2 nanoparticles with IM and PEI were doped into the epoxy matrix and applied on polished steel substrate to form pre and top layers of nanocomposite coatings, respectively. TEM analysis confirms the almost globular morphology of the zirconia nanoparticles with a particle size of 15–25 nm. The chemical bonding interactions among various species were confirmed through FTIR. The synergistic effect of self-healing agent and corrosion inhibitor in epoxy-based double-layer nanocomposite coatings demonstrated the pH and time dependence release of inhibitor and self-healing agent. A comparative EIS analysis conducted in 3.5 wt% NaCl solution reveals that epoxy-based double-layer nanocomposite coatings demonstrate improved corrosion resistance performance as compared to the blank epoxy and single layer epoxy reinforced coatings. This enhanced corrosion resistance of epoxy-based double-layer nanocomposite coatings can be ascribed to the efficient release of loaded IM and PEI in response to the external stimuli and can be potentially considered to circumvent corrosion in oil & gas and marine applications.

1. Introduction

The utilization of polymeric coatings is the most advanced approach to protect steel from destructive corrosion phenomena

* Corresponding authors.
E-mail addresses: ramazank@qu.edu.qa (R. Kahraman), shakoor@qu.edu.qa (R.A. Shakoor).

https://doi.org/10.1016/j.matdes.2021.109839
0264-1275/

[1]. Polymeric coating not only provides a barrier against corrosive species such as oxygen, water, Cl^-, H^+ ions but also works as a matrix to accommodate numerous corrosion inhibition species to provide active corrosion protection [2]. However, these coatings are more prone to the attack of water, oxygen, and ions due to their permeability, which eventually leads to the diffusion of corrosive species into the coatings and poor adhesion with the substrate, thus facilitating the propagation of corrosion [3,4] Currently, polymeric nanocomposite coatings gained more attention due to enhanced thermal, mechanical, physical and barrier properties, achieved by the addition of nanofillers into the polymeric coatings [5,6]. Among various factors to be considered for promising barrier protection, homogenous dispersion of nanofillers and their compatibility with the matrix must be ensured [7,8]. A wide variety of inorganic nanofillers is extensively reported in the literature that has resulted in exceptional corrosion protection. Several reported inorganic nanofiller are Titania oxide (TiO_2) [9-13], Silica (SiO_2) [12,14,15], Ceria (CeO_2) [16-19], halloysite nanotubes (HNTs) [20-24] Carbon nanotubes (CNTs) [25,26], Talc nanoparticles (TNPs) [27,28], layer double hydroxides (LDH) [29-31], Zirconia (ZrO_2) [32,33] and Zinc oxide (ZnO) [34].

Zirconia (ZrO_2) nanoparticles are reported to be the most promising nanofillers employed for active corrosion protection. ZrO_2 possesses excellent mechanical, physical, and chemical properties [35–38]. ZrO_2 nanoparticles also offer improved wear and corrosion resistance and better adhesion to the metal substrate. Moreover, the chemical stability of ZrO_2 nanoparticles makes them an excellent candidate for metallic substrate coating [39]. Due to such outstanding properties, ZrO_2 nanoparticles can be utilized as a carrier for many functional species such as corrosion inhibitors and self-healing agents. It is pertinent to note that functional species are not usually directly added to the polymeric coatings due to their undesirable reactions with matrix eventually leading to the coating degradation and decrease in coating inhibition efficiency [40].

The latest literature is rather useful with lots of inputs focusing on the modification of nanocarrier with functional species, which resulted in superior corrosion protection of steel substrate. Wenhua Xu et al. [41] studied the corrosion inhibition performance of nano-ZrO_2 in phenolic-epoxy resin in hot mixed acid solution employing electrochemical impedance spectroscopic technique (EIS). The results demonstrated that coatings were modified by 1 and 3 wt% nano-ZrO_2 showed better corrosion inhibition efficiency compared to the ones modified by 5 wt% nano-ZrO_2. Lv, Xinding et al. [33] synthesized a hybrid nanocarrier by sandwiching reduced graphene oxide (rGO) between ZrO_2 nanoparticles via the self-assembly method to synthesize GZ. These hybrid nanocarriers were incorporated into an epoxy-based matrix. EIS results revealed the excellent corrosion inhibition efficacy in 3.5 wt% NaCl solution. Arunchandran Chenan et al. [42] synthesized hollow mesoporous (hm) ZrO_2 nanoparticles via hard template method utilizing SiO_2 as a template. Hm-ZrO_2 particles were then modified by 2-MBT (2-Mercaptobenzothiazole) as a corrosion inhibitor. UV–vis spectroscopic analysis results demonstrated the successful loading and release of the inhibitor from the hm-ZrO_2 carrier. Ge Tianhao et al. [43] designed alternative epoxy-rGO/ epoxy zinc multi-layered coating to study the corrosion inhibition effect for Cu. They evaluated the protection potential of the anti-corrosion coatings and substrate utilizing long-term electrochemical tests in different wt. % NaCl solution. It was revealed that the coating with a double-layer structure retains the extended electrochemical protection ability and exceptional adhesion potential under a severe environment, thus providing insights on the application of coatings with a new multi-layered structure. E. Salahinejad et al. [44] explored the corrosion protection ability of the double layer $ZrTiO_4$ (bottom layer) and $ZrTiO_4$-PMMA (top layer) coatings. For that purpose, the medical graded stainless-steel substrate was coated via sol–gel spin coating method. According to the results obtained from the potentiodynamic polarization experiments, the substrate coated with a double layer exhibited superior corrosion protection in simulated body fluids as compared to those coated with pure $ZrTiO_4$ and hybrid $ZrTiO_4$-PMMA film. Kim, Heejin et al. [45] developed double layer coatings to elucidate the corrosion inhibition performance in marine environment. Self-healing bromobutyl Rubber (BIIR) film was deposited as top layer and CNT/BIIR film was deposited as bottom layer. The films were prepared by drop casting, spraying, or painting of BIIR solution. Joule heating of the CNT/BIIR film assisted to heal the defect site in the BIIR layer in few hours. The prepared double layer coatings also helped in corrosion protection in marine environment.

In this work, we reported the corrosion behavior of epoxy-based double-layer (pre and top-coat) nanocomposite coatings applied on steel substrates which were obtained by reinforcing epoxy matrix with modified ZrO_2 nanoparticles (nanocarriers) with corrosion inhibitor (imidazole-IM) and self-healing agent (polyethyleneimine-PEI)). The successful loading of corrosion inhibitor and self-healing agent into ZrO_2 nanocarriers was confirmed by transmission electron microscopy (TEM), Energy Dispersive X-Ray Analysis (EDX), and UV–vis spectroscopy. The chemical interaction and thermal stability of modified ZrO_2 nanoparticles were achieved by utilizing Fourier-transform infrared spectroscopy (FTIR) and thermogravimetric analysis (TGA) respectively. Phase changes before and after modification of ZrO_2 were achieved by X-Ray Diffraction Analysis (XRD) analysis. Self-release of functional species was validated through UV–vis spectroscopy at acidic and basic pH medium. The corrosion inhibition efficiency of the double-layer epoxy-based nanocomposite coatings was evaluated by employing the EIS technique in 3.5 wt% NaCl solution. The results demonstrate that double-layer nanocomposite coatings demonstrate improved corrosion resistance performance as compared to the blank epoxy coatings and single layer epoxy reinforced coatings. This enhanced corrosion resistance of epoxy-based double-layer nanocomposite coatings can be ascribed to the efficient release of loaded IM and PEI into the ZrO_2 nanoparticles in response to the external stimuli (crack and pH change). The promising corrosion protection ability of double-layer nanocomposite coatings makes them attractive for oil & gas and marine applications.

2. Experimental section

2.1. Chemicals used

As-received Zirconia nanoparticles (ZrO_2) utilized as nanocarriers, imidazole (IM), used as the corrosion inhibitor, Polyethyleneimine (PEI, branched average molecular weight ~ 25,000), used as the self-healing agent, epoxy resin (815C), and its curing agent (EPIKURE curing agent 3282), hydrochloric acid, sodium hydroxide pellets were procured from Sigma Aldrich, Darmstadt. Carbon steel coupons ($30 \times 30 \times 1.0$ mm^3) utilized as substrates were acquired from a local source. Silicon carbide (SiC) abrasive papers were obtained from Hebei Yineng Pipeline Group Co., Ltd, China.

3. Modification of ZrO_2 nanoparticles with IM and PEI

The modification of as-received ZrO_2 nanoparticles with corrosion inhibitor (IM) was initiated by the formulation of a saturated solution of IM in the corresponding solvent (water). After preparing the IM solution, nanoparticles were added in the ratio of 2:1. This solution was then stirred for 24 h at room temperature. After stirring it was placed into a vacuum chamber for another 24 h by alternative vacuuming and de-vacuuming cycle to validate the removal of air entrapment and proper loading of IM into ZrO_2 nanoparticles. The solution was then centrifuged for 20 min at 5000 rpm to get the final product, followed by complete drying at 60 °C overnight. The final modified ZrO_2-IM particles were then grounded in pastel to get fine particles (Fig. 1a). The same procedure of loading of PEI (self-healing agent) into ZrO_2 was followed as that of IM, which resulted in the synthesis of ZrO_2-PEI nanoparticles. (Fig. 1b).

4. Characterization of unmodified and modified ZrO_2 (ZrO_2-IM and ZrO_2-PEI) nanoparticles

Fourier transform infrared spectra were conducted using FTIR Frontier (PerkinElmer, Waltham, MA, USA) spectrometer in the range of 4000–500 cm^{-1} to study the bonding interactions between different species present in the modified ZrO_2 nanoparticles. The microstructural analysis of the modified ZrO_2 nanoparticles was performed by transmission electron microscopy (TEM, FEI, TALOS F200X, USA). The composition of the modified ZrO_2 nanoparticles was estimated with energy dispersive X-Ray spectroscopy (EDX). The Brunauer-Emmett-Teller-BET (Surface Area Analyzer, Micromertitcs ASAP 2420, USA) was employed to study specific surface area and cumulative pore volume of unmodified and modified ZrO_2. Thermal stability of unmodified and modified ZrO_2 was conducted using TGA analyzer pyris 4000 (PerkinElmer-USA) ranging from 30 to 600 °C at the heating rate of 10 °C/min. To confirm the loading of IM/ PEI and their release from modified ZrO_2 nanoparticles at different pH values, UV–Vis spectroscopic analysis (Biochrome Libra S60 double beam spectrophotometer, United Kingdom) was performed. For this purpose, a small amount (0.5 mg) of modified ZrO_2 was added into 6.0 ml of 0.1 M NaCl solution to form a suspension. The pH of the solution was adjusted to 2, 5, 7, 9, and 11 by adding suitable amounts of either HCl or NaOH, and the released amount of IM and PEI was plotted as a function of time.

5. Preparation of steel substrate

As-received steel substrate was polished employing a grinding and polishing machine (Metkon ForcoPol IV) utilizing SiC abrasive papers (120-2c and 220-2c). The polished steel substrates were then cleaned with acetone to remove any residue and then coated with blank and reinforced epoxy coatings.

6. Development of epoxy reinforced with modified ZrO_2 nanocomposite coatings.

Four different types of coatings were developed, labelled as (i) blank epoxy, (ii) epoxy reinforced with ZrO_2 nanoparticles modified with IM (epoxy/ZrO_2-IM), (iii) epoxy reinforced with ZrO_2 nanoparticles modified with PEI (epoxy/ ZrO_2-PEI) and (iv) epoxy-based double-layer nanocomposite coatings (epoxy/ ZrO_2-IM) (Pre-layer)/ (epoxy/ ZrO_2-PEI) (top layer). For blank epoxy coatings, 3 gms of epoxy was mixed with 0.6 gm of hardener and kept for sonication at degasser mode to remove air bubbles from the epoxy mixture. This mixture was then applied on polished steel substrate employing the doctor blade technique and kept for curing at room temperature in closed space. To synthesize epoxy/ ZrO_2-IM coatings, 1 wt% of ZrO_2-IM was added into epoxy and stirred for 10 min and then hardener was added into it, followed by sonication for 10 min to remove air bubbles and left for curing for few days till it is completely cured. A similar method was employed to synthesize epoxy/ZrO_2-PEI coatings. To develop (epoxy/ ZrO_2-IM)/ (epoxy/ ZrO_2-PEI) nanocomposite coatings, the cleaned steel substrates were coated with thin epoxy/ ZrO_2-IM pre-layer (100 ± 5 μm) and then top-coated with epoxy/ ZrO_2-PEI top layer (100 ± 5 μm) (thickness measured by employing PosiTector 6000) from DeFelsko (Made in the USA). Both layers of reinforced epoxy coatings were modified with 1 wt% modified ZrO_2. The coatings were done utilizing a doctor blade. After applying pre layer, the top layer was applied within 24 h. The coated steel substrates were then left for curing for 2 weeks before the commencement of EIS testing.

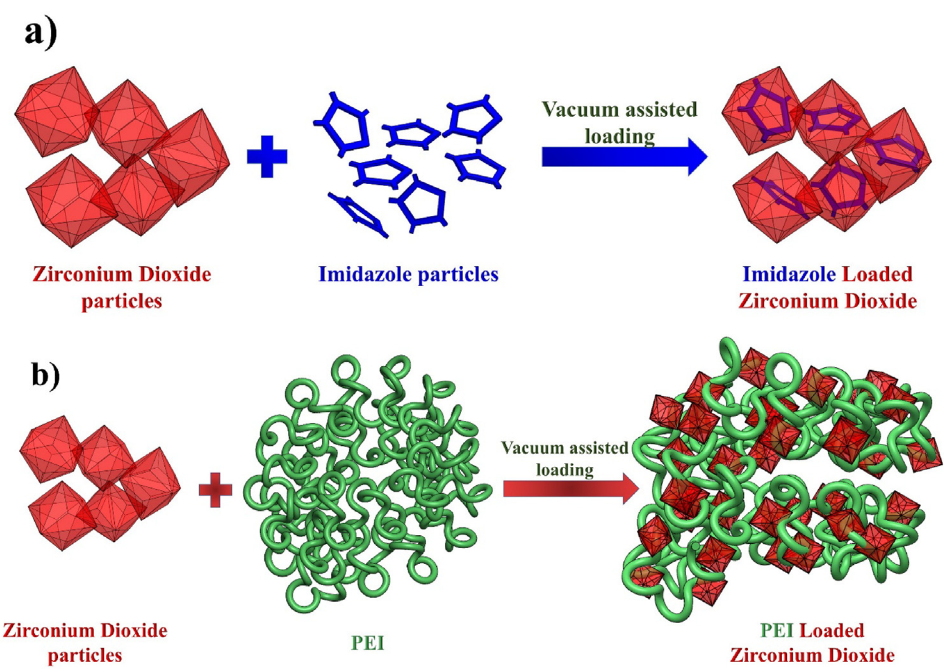

Fig. 1. Schematics showing the modification of a) IM into ZrO_2 b) PEI into ZrO_2.

7. Characterization of epoxy-based nanocomposite coatings

The barrier properties of the synthesized polymeric nanocomposites in 3.5 wt% NaCl solution was analyzed using Electrochemical Impedance Spectroscopy (EIS) technique. For this purpose, the prepared coatings were exposed to artificial damage. A manual scratch of ~ 139 μm width was produced employing a scalpel on the coatings before the EIS evaluation. The electrochemical measurements were recorded using Gamry 3000 (30 K BOOSTER Potentiostat/Galvanstate/ZRA, USA) encompassing a three-electrode system. In this study, the coated sample was utilized as the working electrode, while the graphite rod and Ag/AgCl were employed as the counter and the reference electrodes, respectively. EIS measurements were initiated after attaining the open circuit potential to a steady value. The frequency range for the EIS experiment was within 0.1 Hz –100 kHz from the higher to the lower value, and the RMS signal was 10.0 mV. The measured EIS data were evaluated by Gamry E-Chem 3000 software, and fitting parameters were ascertained by the suitable equivalent circuits. All EIS measurements were performed at room temperature (25 °C).

8. Results and discussion

8.1. Structural and morphological analysis of unmodified and modified ZrO_2

The structure and chemical bonding of unmodified and modified ZrO_2 nanoparticles were analyzed by FTIR analysis as represented in Fig. 2. Pure IM displayed characteristic peaks of C-H stretching vibration in the region of 3124–2912 cm^{-1}, C-C stretching vibrations in benzene derivative aromatic ring in a range of 1672–1548 cm^{-1}, C-N stretching in the region of 1441–1317 cm^{-1}, C-H in and out of plane stretching vibrations in the region of 1254–928 cm^{-1}, N-H out of plane bending at 830 cm^{-1} and ring deformation in and out of plane bending vibrations in the region of 653–615 cm^{-1} [46] as shown in Fig. 2a. Pure PEI represented the characteristic peaks of N-H stretching in the range of 3359–3289 cm^{-1}, C-H symmetric and asymmetric stretching in range of 2950–2834 cm^{-1}, N-H deformation peak at 1638 cm^{-1}, and C-N stretching peak at 1035 cm^{-1} [47] as shown in Fig. 2a. However, the broad absorption band (Fig. 2b) in the range of 3676–2944 cm^{-1} range is due to the stretching vibrations of the OH groups of water molecules [48], while the absorption band which emerged at 1635 cm^{-1} is the characteristic peak of the bending vibration of water molecules. The characteristic bands assigned to the monoclinic phase of zirconia are 583 and 781 cm^{-1} [49] and tetragonal zirconia is 480 cm^{-1} [50]. The peak at 665 cm^{-1} is also attributed to monoclinic ZrO_2 as represented in Fig. 2b [51].

In the case of ZrO_2 modified with IM, the similar peaks of C-H stretching are seen in a range of 3108–2612 cm^{-1} and of benzene derivative aromatic ring C-C stretching vibrations band in the range of 1328–1054 cm^{-1}. This displacement in the wavenumbers of peaks of IM is ascribed to be due to the physical bonding that takes place between ZrO_2 and IM as shown in Fig. 2b. In the case of ZrO_2 modified with PEI, the peaks of C-H symmetric stretching are displaced to 2811 cm^{-1}, N-H deformation peak is displaced to 1638 cm^{-1} and C-H deformation peak is seen at 1467 cm^{-1} after loading due to the bonding between PEI and ZrO_2 as shown in Fig. 2b.

The transmission electron microscopy (TEM) and EDX analyses of modified ZrO_2 nanoparticles are represented in Fig. 3. For a full comparison purpose, TEM and EDX analyses of unmodified ZrO_2 nanoparticles are also presented. Most unmodified ZrO_2 nanoparticles (Fig. 3a) exhibit a uniform polygonal shape that is close to spherical morphology with an average particle size of 15–25 nm. The EDX analysis confirms that the main elements of ZrO_2 (Zr, O) are appeared in the analysis (Fig. 3b) confirming its phase purity. The TEM analysis of modified ZrO_2-IM (Fig. 3c) and ZrO_2-PEI (Fig. 3e) represented that there is no major change in the morphology of the product, however, a bit more agglomeration after loading of the corrosion inhibitor and self-healing agent can be noticed. EDX analysis confirms the loading and physical interaction of IM and PEI with ZrO_2 as the main constituents of IM and PEI (C, N, O) are seen in the EDX spectra (Fig. 3d, f). According to these results, the weight % of Zr is 15.37% for unmodified ZrO_2 nanoparticles which is reduced to 5.06 and 8.89% in the ZrO_2 modified with IM and PEI, respectively. The reduction in the weight % of Zr in the modified ZrO_2 could occur because of the insertion of C, N, O atoms of IM and PEI in the original structure of the ZrO_2 nanoparticles.

The isotherm of the Brunauer-Emmett-Teller (BET) demonstrating the specific surface areas of the unmodified ZrO_2 and modified ZrO_2 nanoparticles are displayed in Fig. 4, with an inset demonstrating cumulative pore volume. The specific surface area (SSA) of the unmodified ZrO_2 is revealed to be 66.310 m^2g^{-1}, and the cumulative pore volume is calculated to be 0.474970 ccg^{-1}. The BET measurements of the ZrO_2 modified with IM indicate that the SSA is decreased to be 52.372 m^2g^{-1} and that of ZrO_2 modified with PEI is decreased to 49.289 m^2g^{-1}. Besides, the pore volume is also reduced to 0.428173 and 0.408007 ccg^{-1} respectively, revealing the loading of the inhibitor IM and self-healing agent PEI into

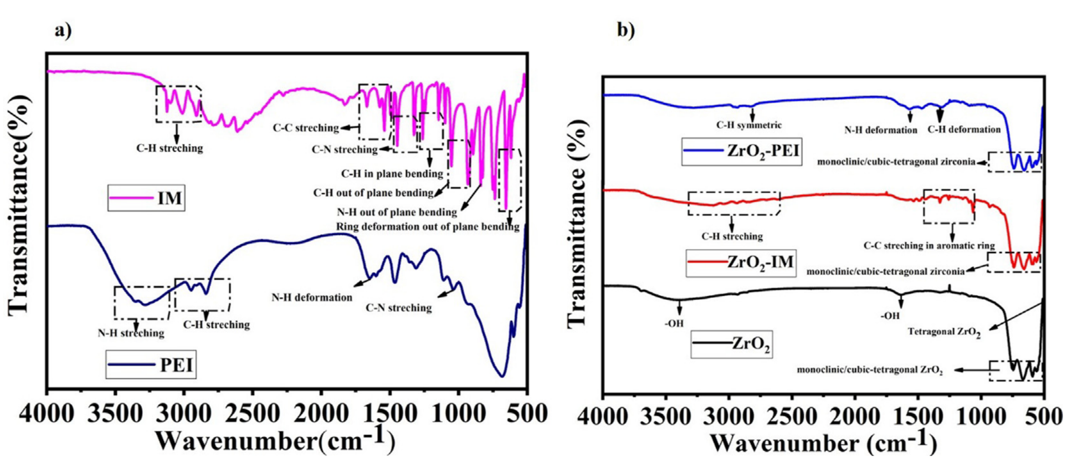

Fig. 2. FTIR analysis of (a) Pure IM and PEI (b) Unmodified ZrO_2 and modified ZrO_2 with IM and PEI.

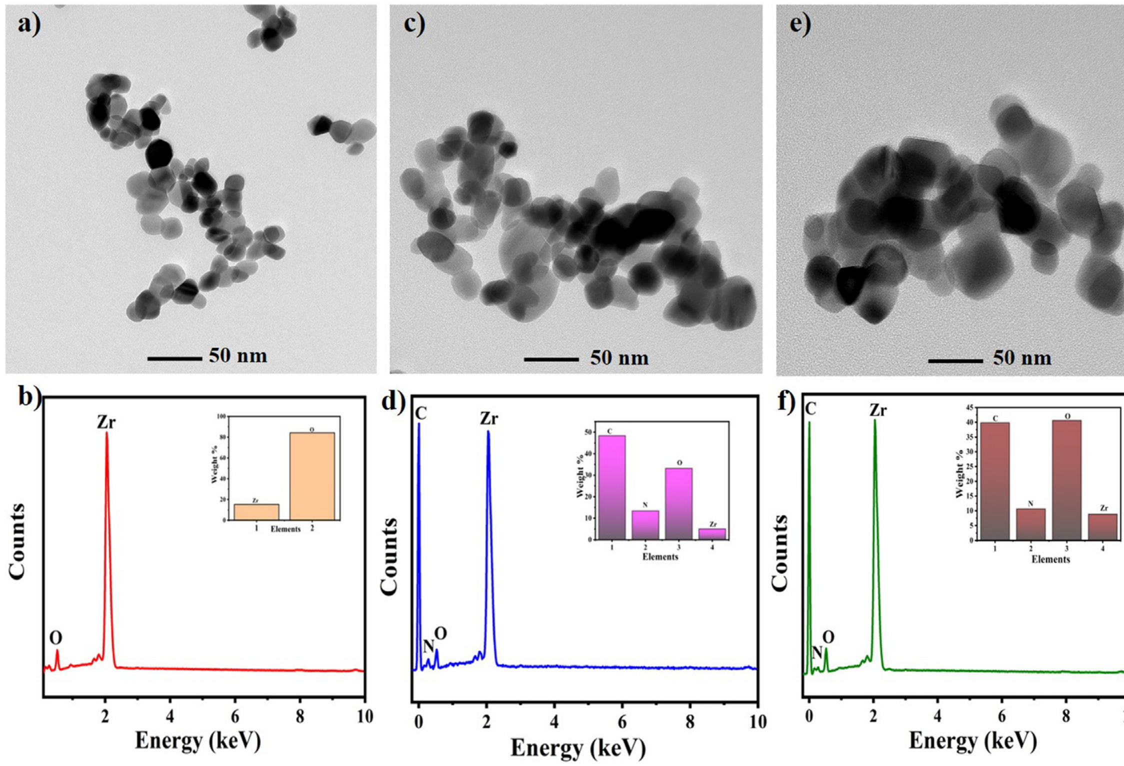

Fig. 3. TEM and EDX analysis of (a, b) Unmodified ZrO_2, (c, d) ZrO_2 modified with IM, and (e, f) ZrO_2 modified with PEI.

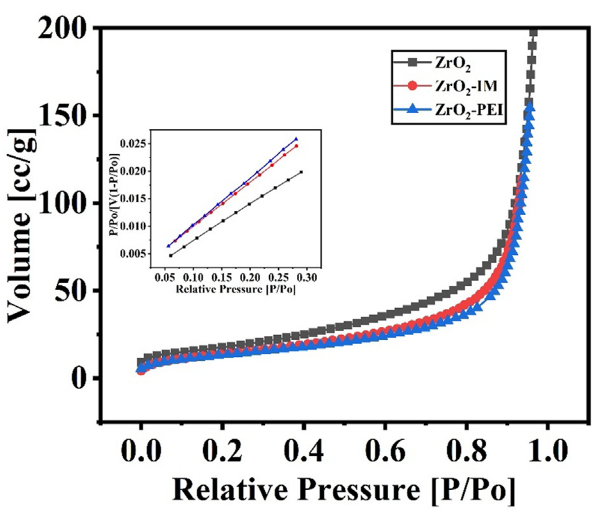

Fig. 4. BET analysis of unmodified ZrO_2 and modified ZrO_2 with IM and PEI.

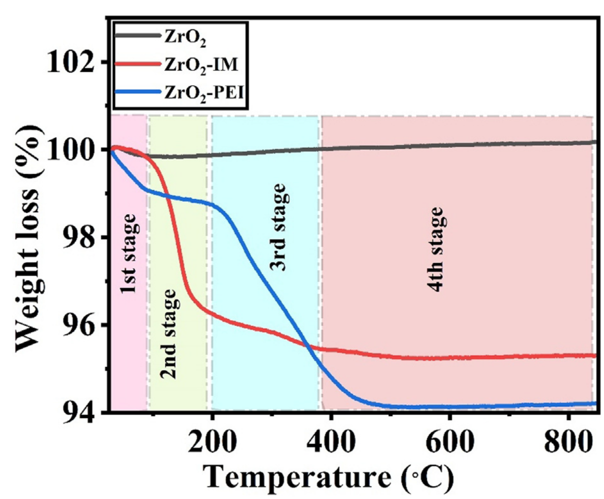

Fig. 5. Thermal stability analysis of unmodified ZrO_2, modified ZrO_2 (ZrO_2-IM, ZrO_2-PEI).

ZrO_2. These findings are consistent with previous studies [52] that the modification or functionalization of nanoparticles leads to a decreased in specific surface area and pore volume.

8.2. Thermal stability analysis of unmodified and modified ZrO_2

TGA analysis of unmodified and modified ZrO_2 nanoparticles is shown in Fig. 5. A straight line in the TGA curve of unmodified ZrO_2 nanoparticles is an indication of the high thermal stability of ZrO_2 nanoparticles (melting point = 1855 °C). A negligible weight loss ~ 0.5% in the TGA analysis of unmodified ZrO_2 nanoparticles may be ascribed to the presence of moisture contents. In the case of ZrO_2-IM nanoparticles, the weight loss can be divided into four stages. In the first stage, there is only ~ 1% of weight loss which is due to the removal of moisture in the product. The major degradation peak of weight loss is seen in the second stage which is associated with the decomposition of IM, as the melting point of imidazole is around 91 °C. IM starts to decompose at ~ 88 °C and is completely decomposed at 187 °C. Similar behavior of IM is also observed in the previous reports [21]. This increase in the decomposition temperature of IM is showing the successful loading of IM into ZrO_2. About 4% of weight loss is noticed in this region. In the third stage, again ~ 1% of weight loss is seen which can be attributed to the removal of water molecules. In the fourth stage, the ZrO_2-IM nanoparticles are appeared to be stable even after 800 °C which is due to the thermal stability of ZrO_2. In the case of ZrO_2-PEI, the weight loss is also in four stages. The initial 2% of weight loss in the first and second stage is because of moisture content in the product. The major decomposition peak is seen in the third stage, demonstrating the breakdown of PEI long polymeric chains, as PEI started to decompose at 198 °C and completely decomposed at 387 °C. Similarly, as in the case of IM high decomposition temperature of PEI is demonstrating the successful loading of PEI into ZrO_2. Almost 4% of weight loss is seen in the third stage. After this stage, the weight loss is almost constant showing the high thermal stability of ZrO_2. TGA analysis of modified ZrO_2 nanoparticles indicates the successful loading of IM (5.26 wt%) and PEI (6.38 wt%) into the ZrO2 nanoparticles calculated from ratio mass loss calculations [16].

8.3. pH-sensitivity of modified ZrO_2 nanoparticles

The self-release behavior of inhibitor (IM) and self-healing agent (PEI) from modified *ZrO_2 nanoparticles* was studied employing UV–vis spectroscopy. The modified ZrO_2/IM and ZrO_2/PEI nanoparticles were separately mixed in 0.1 M NaCl solution and then different solutions with varying pH values (2, 5, 7, 9, 11) were prepared by adjusting the pH solutions. The UV spectra of ZrO_2/IM and ZrO_2/PEI nanoparticles were studied as a function of time for consecutive four days, as shown in Fig. 6 (a, b). In the case of ZrO_2 modified with IM, different distinct absorption bands have appeared. The main absorbance band obtained at 211 nm corresponds to the π-π^* transition and absorption bands at 236 and 270 nm corresponds to the n-π^* transitions of the aromatic ring in IM [21,53]. Though IM represented release at all pH values, the release of IM is more pronounced in pH 2 and 5 which is an acidic medium. In sodium chloride solution, the solution has an excess of Cl^- ions. In an acidic medium (pH 2, 5), the nitrogen atom in the aromatic ring of IM of the inhibitor can be easily protonated due to high electron density which leads to the formation of positively charged inhibitor species. The adsorption can occur via electrostatic interaction between positively charged inhibitor molecules and negatively charged Cl^- ions [54]. There is a slight difference in intensity at different time intervals indicating an increasing trend. In this way, more amount of released inhibitor will be available an acidic medium to minimize the corrosion rate. The release of IM at pH (2, 5) demonstrates that IM is sensitive to acidic pH as compared to neutral and basic pH.

Similar behavior has been observed in the case of PEI. The main absorbance peak is observed at 205 nm which is attributed to the π-π^* transition of the N-H bond [55]. The PEI demonstrates more sensitive behavior towards the acidic medium as compared to the basic medium. As explained above, PEI also represents better and more efficient release in the acidic medium due to the protonation of secondary amine in the structure [56]. The release of PEI is also affected by time as with time the intensity of absorption peak is also increasing in all mediums. It can be assumed that in an acidic medium, both IM and PEI provide an effective self-release allowing promising corrosion protection.

8.4. Self-healing analysis of double-layer nanocomposite coatings

The main function of self-healing coating is to provide healing or repair of the damaged area due to the change in the external stimuli (pH, moisture, temperature). To analyze self-healing ability of epoxy-based double-layer nanocomposite coatings (epoxy/ ZrO_2-IM)/ (epoxy/ ZrO_2-PEI) over the 7 days, SEM analysis was done. The epoxy-based double-layer nanocomposite coatings were carefully scratched manually utilizing a scalpel. After that, a drop of 3.5 wt% NaCl solution was dropped on the scratch area and dried the surface after some time. The samples were fixed with conducting tapes to ensure the in-situ observation before and after healing. The healing is achieved due to the release of PEI from modified ZrO_2 nanoparticles (ZrO_2/PEI) from the top layer which resulted in the self-healing of the damaged area. The release of PEI is sensitive to mechanical damage and localized change in pH. The presence of PEI improves the cross-linkage density of the epoxy coating, which also decreased the intrinsic defects of the coating. Also, PEI supports the dispersion of ZrO_2 nanoparticles in the epoxy coating, which is useful to utilize the physical barrier efficacy of nanoparticles. In short, the homogeneous integration of ZrO_2/PEI in the epoxy coating has prevented the pathway for corrosive medium (O_2, H_2O, and $Cl^{-)}$, which can reduce the occurrence of local corrosion of metal substrate [57]. The combined effect of PEI as a self-healing agent and IM as corrosion inhibitor resulted in overall corrosion inhibition performance of coatings as shown in Fig. 7a. The EDS analysis (Fig. 7b) also confirms the presence of main elements of PEI and IM (C, O, N) at the damaged area which confirmed the formation of a protective passive layer. The presence of the small amount of Fe is from metal steel substrate and Cl is due to the NaCl solution. As shown in Fig. 7 (a), at day 1 the initial scratch diameter was ~ 133 µm which is decreased to ~ 51.9 µm after 7 days displaying self-healing efficiency of ~ 81%.

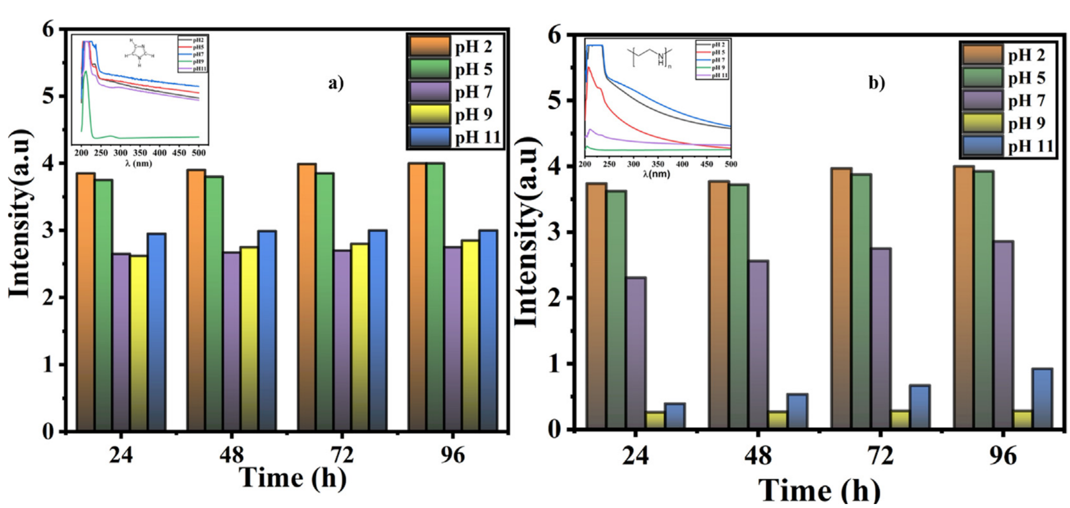

Fig. 6. UV–VIS spectroscopic analysis of a) ZrO_2/IM and b) ZrO_2/PEI in different pH solutions (2, 5, 7, 9, and 11) at different time intervals (24, 48, 72, and 96 h) in 0.1 M NaCl solution.

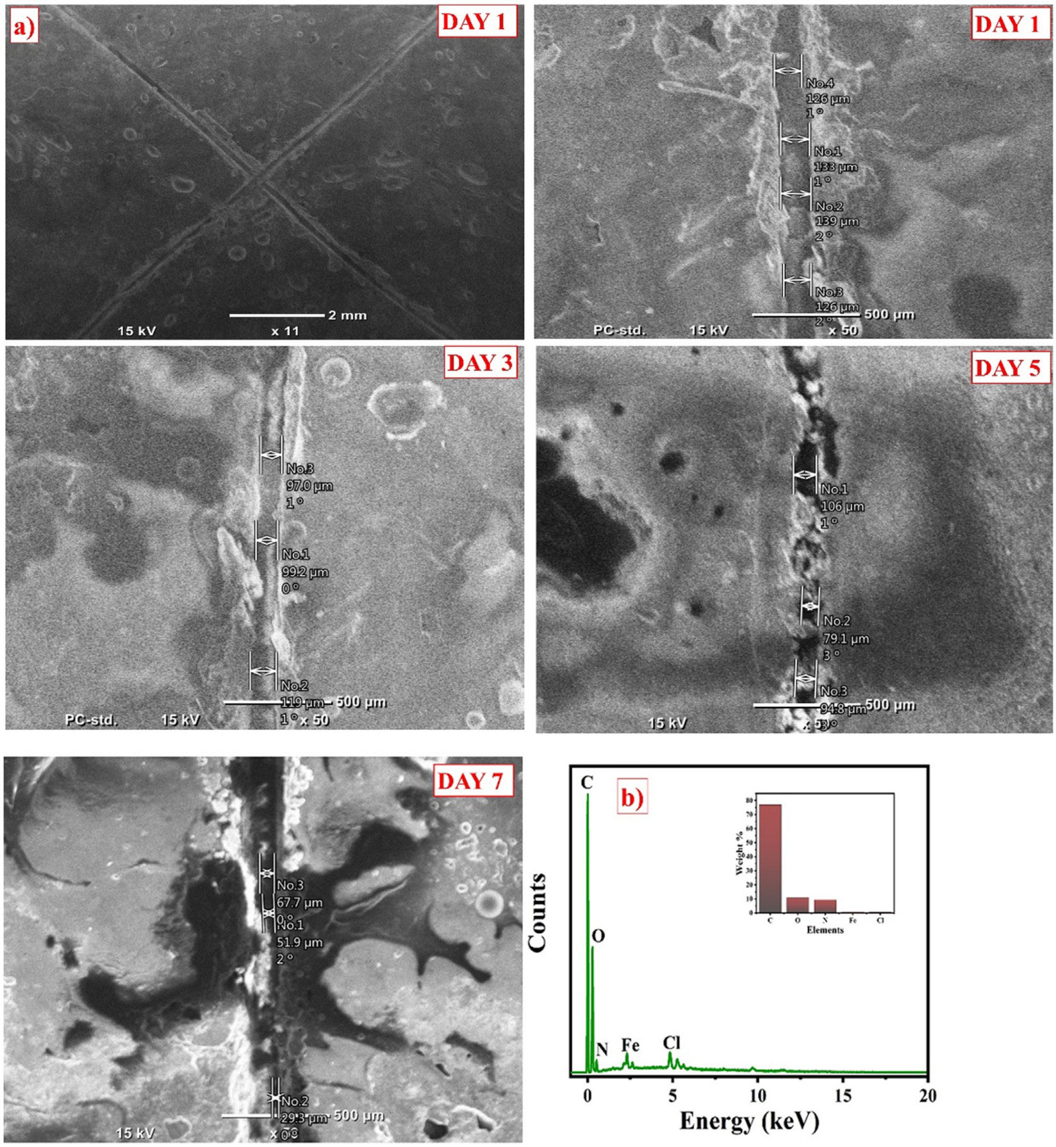

Fig. 7. (a) SEM micrographs of scratched epoxy based double-layer nanocomposite coatings demonstrating self-healing performance over 7 days (b) EDX analysis of passive layer formed on the scratched area of the developed epoxy based double-layer nanocomposite coatings.

9. Corrosion inhibition performance

9.1. EIS of epoxy-based double-layer nanocomposite coatings

The corrosion inhibition performance of blank epoxy, epoxy-based single layer (epoxy-ZrO_2/IM, epoxy-ZrO_2/PEI) and double-layer nanocomposite coating was evaluated by EIS technique after 1, 3, 5, and 7 days of immersion in 3.5 wt% NaCl solution. The bode and phase angle plots acquired after different immersion times for tested coatings are represented in Fig. 8. The obtained electrochemical data were fitted by two equivalent circuits with one and two times constant for blank epoxy and reinforced epoxy coatings respectively as shown in Fig. 10. In the equivalent circuit the R_s, R_{po}, R_{ct}, and W are the solution resistance, pore resistance, charge transfer resistance, and Warburg diffusion constant respectively which is used to represent the mass diffusion at a low-frequency range. The CPE_1 and CPE_2 are associated with the coating and double-layer constant phase elements, correspondingly. The constant phase elements are used to represent the non-ideal capacitance behavior of the metal surface because of the surface heterogeneity which is due to the adsorption of functional species on the metal substrate, formation of the passive protective layer, and surface roughness on the metal surface [58]. The R_{po}/CPE_1 is associated with the polymeric coating properties and R_{ct}/CPE_2 is correlated to the coating barrier properties. The impedance of CPE is computed using the given Equation [59];

$$Z_{CPE} = \frac{1}{Y_0(jw)^n} \tag{1}$$

where Y_0 represents the admittance ($s\Omega^{-1}$ cm^{-1}), j is an imaginary number $(-1)^{1/2}$, x demonstrates the angular frequency of the AC signal (1/rad), and n is the CPE exponent, and its value ranges from 0 to1. When n reaches 1, the CPE demonstrates the ideal capacitor behavior, and resistor behavior is observed when n = 0.

The bode and phase angle plots for the blank epoxy coatings at different time intervals (1, 3, 5, 7 days) are represented in Fig. 8. The impedance value on the first day of immersion is 10^5 $\Omega.cm^2$ at a low-frequency range of $|Z|_{0.1Hz.}$ This impedance is associated with the coating barrier properties. The impedance of blank epoxy coating continued to decrease over the period and on the 7th day of

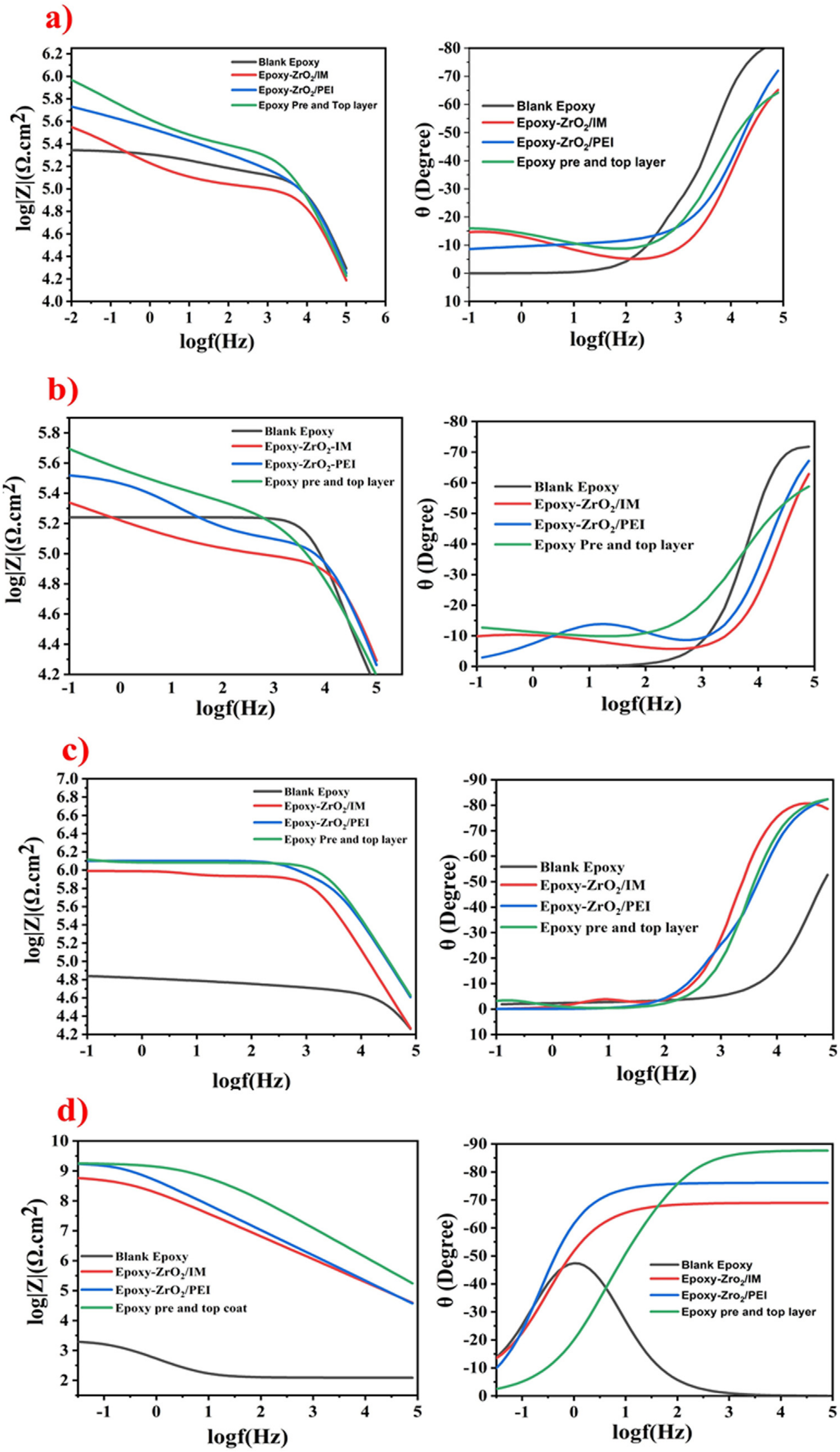

Fig. 8. Bode and Phase angle plot a) after 1 day of immersion, b) after 3 days of immersion (c) after 5 days of immersion, (d) after 7 days of immersion for the blank epoxy and epoxy based nanocomposite coatings.

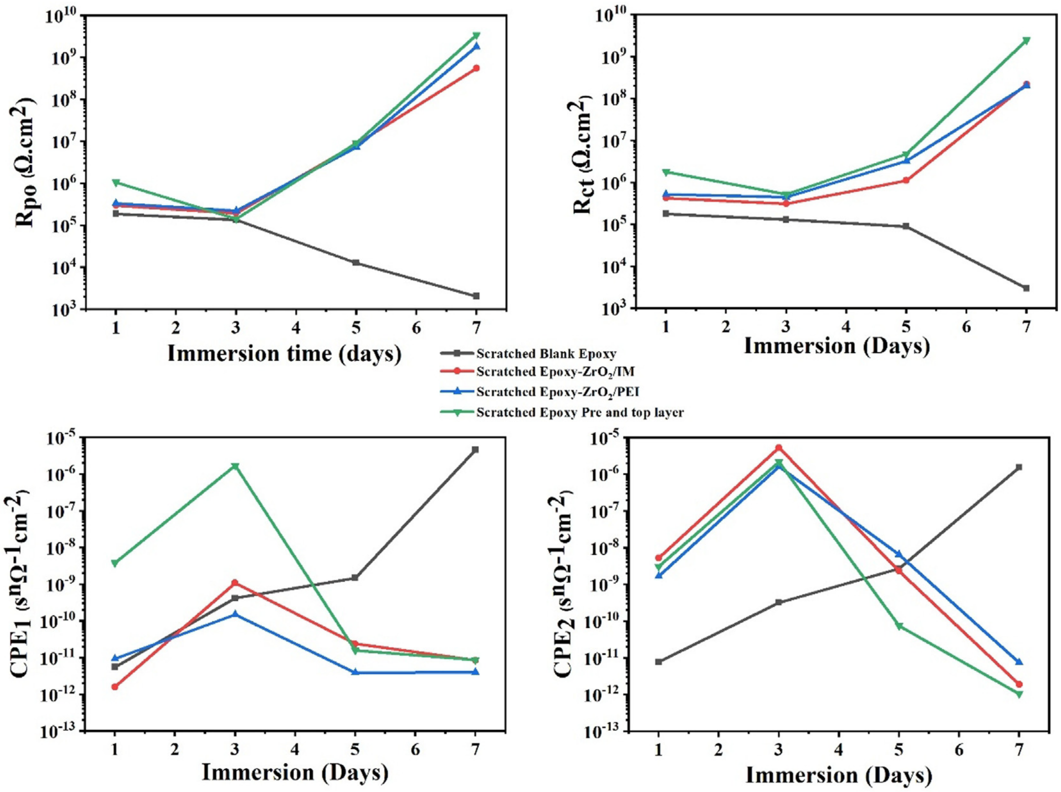

Fig. 9. Variation of coating pore resistance R_{po}, charge transfer resistance of the coatings R_{ct}, the value of the capacitance CPE_1, and value of the capacitance CPE_2 at different time intervals of immersion in 3.5 wt% NaCl solution.

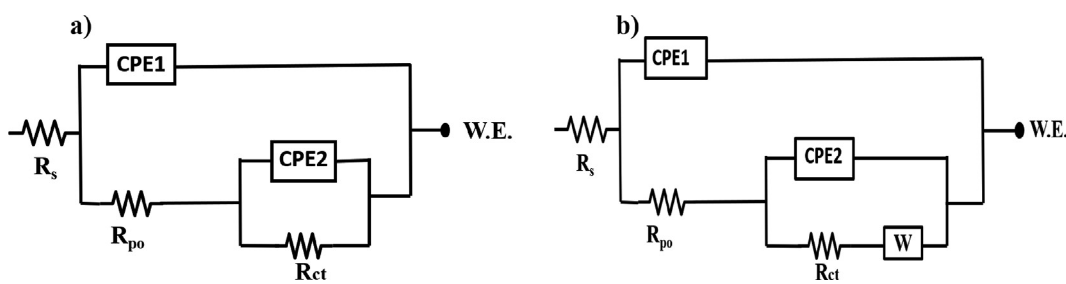

Fig. 10. Equivalent circuit used to fit data a) Blank epoxy coatings b) Epoxy based nanocomposite coatings modified with ZrO_2 nanoparticles (single layer and double layer).

immersion, it reached 10^3 Ω.cm^2. The phase angle is seen to be below −10° on the 7th day of immersion. This decrease in phase angle from −80° on the 1st day to −10° on the 7th day of immersion represents the negligible capacitance behavior of blank epoxy coatings, which may lead to the de-adhesion of coating and poor barrier properties. The performance of blank epoxy coatings deteriorated due to the diffusion of electrolyte into the epoxy-steel interface thus leading to the formation of corrosion products and progression of the corrosion process [60].

In the case of epoxy-based ZrO_2/IM single-layer nanocomposite coatings, the impedance values at low-frequency range $|Z|_{0.1Hz}$ represent the effective corrosion inhibition performance as shown in Fig. 8. The impedance value on the 1st day of immersion is 10^5 Ω.cm^2, but after the 3rd day of immersion, it reveals a decrease which is due to the diffusion of electrolyte, thus propagates the corrosion activity. This eventually changes the pH at the scratched area which triggered the release of IM from the ZrO_2 nanoparticles and thus facilitates the formation of the passive protective layer. The detailed healing mechanism will be discussed in section 3.5.2 and Fig. 11. On the 5th day of immersion, the low-frequency impedance exhibits an increase in values which demonstrates an improved corrosion inhibition protection. The phase angle exhibits the two capacitance loops and is close to −80° which represents the capacitance behavior of the coatings. The epoxy-based ZrO_2/PEI single layer coatings represent the same behavior as in the case of ZrO_2/IM but the impedance values display slightly incremental behavior. This is because of the self-healing of the scratched area as represented in section 3.4 and Fig. 7. The self-healing of the scratch further prevented the progression of the corrosion process as compared to ZrO_2/IM because the leaching out of all the inhibitor from ZrO_2 nanoparticles after some time may have resulted in the decrease in the content of the inhibitor. The phase angle represents the same capacitance behavior of the coatings. The equivalent circuit used to fit the data is represented in Fig. 10.

The epoxy-based double-layer nanocomposite coatings having ZrO_2/IM (pre-coat) and ZrO_2/PEI (topcoat) exhibit better corrosion protection as compared to the rest of the coatings. The impedance values for the double-layer coatings are higher as compared to the

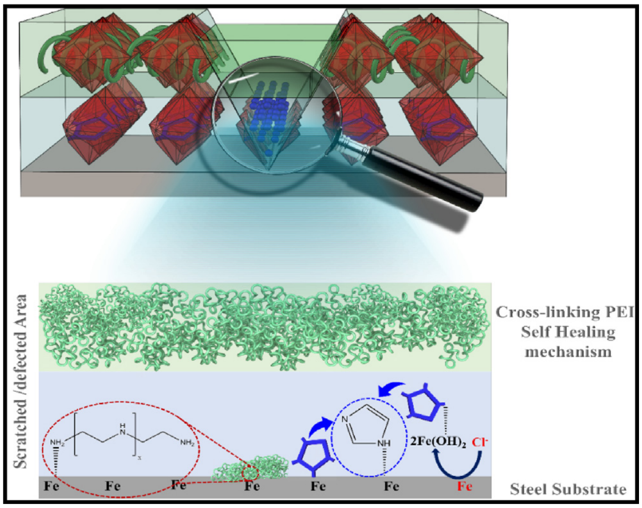

Fig. 11. Schematic diagram demonstrating the self-healing and corrosion inhibition mechanism of the developed epoxy-based double-layer ZrO_2 modified nanocomposite coatings.

single-layer doped and blank epoxy coatings. After 1st day of immersion, the impedance value is 10^6 $\Omega.cm^2$ which increases to 10^9 $\Omega.cm^2$ due to the synergistic effect of corrosion inhibitor and self-healing agent in each layer in double-layer coating. The phase angle after 7 days of immersion is close to $-90°$ which demonstrated the capacitance behavior, good barrier properties, and good adhesion of the coating on the steel substrate. The blank epoxy coatings posses' pores and free volumes which are pathways for the diffusion of electrolyte, but the reinforced epoxy coatings block those pathways for further electrolyte diffusion, also due to the release of functional species (IM and PEI) at the scratched area, the corrosion rate is reduced.

The evolution of R_{po}, R_{ct}, CPE_1, and CPE_2 of all coatings immersed for a different period in 3.5 wt% NaCl solution is represented in Fig. 9. The table displaying all the electrochemical values obtained from fitting data is represented in Table 1. The decreasing trend for both R_{po} and R_{ct} in the case of blank epoxy coating represents the deterioration of coatings. The increase in the CPE_1 and CPE_2 values is the reveals that coating has been damaged due to corrosion and thus leads to poor barrier properties. But in the case of the epoxy-based nanocomposite, the R_{po} and R_{ct} values represent the increasing trend after 3 days of immersion, demonstrating the good barrier properties and better corrosion protection of steel substrate. The R_{po} and R_{ct} values in the case of double-layer nanocomposite coatings are much higher as compared to the epoxy-based single-layer coating due to the synergistic effect of IM and PEI. The decreasing trend of CPE_1 and CPE_2 values is also an indication of good coating barrier properties and adhesion on a steel substrate. A comparison of corrosion protection efficiency of smart coatings developed in this study and reported in the literature is provided in the supplementary data as Table S1. The comparative analysis demonstrate that the reinforcement and coating strategy implemented in this study has resulted in improved corrosion protection as compared to other reported smart coating systems. This enhanced corrosion inhibition performance can be attributed to the synergistic effect of the self-healing agent and inhibitor loaded into smart carrier reinforced into epoxy matrix in pre and topcoat. This double layer coating provided independent and simultaneously self-healing and corrosion inhibition protection to the steel substrate exposed to the 3.5 wt% NaCl solution environment. This increased corrosion protection provided great prospect for its application on oil and gas industry.

9.2. Self-healing and corrosion inhibition mechanism

The possible self-healing and corrosion inhibition mechanism can be described as follow. The inhibiting properties of amines are associated with the ability of the amino groups to adsorb on metals by contributing their unshared electron pair of the nitrogen atom with the metal substrate, thus covering the scratched area on a metal surface (passive film formation) [61,62]. The nitrogen atom (:N) in the amino group ($-NH_2$) is an electron acceptor that can form a bond to a hydrogen atom of a chemisorbed water molecule at the metal surface. The water molecule then desorbs, and its spot will be substituted by another chemisorbed amino group in the case of a self-healing agent. In the case of IM molecules, both two nitrogen atoms in the ring have free electron pairs that can coordinate with the vacant orbits of the steel surface to form a chemosorbed first layer [63]. The most important reaction in the corrosion process instigated due to interaction of steel with Cl, which precedes the development of Fe^{2+}, can be explained by a set of Equations below, demonstrated by the following reactions [64].

$$Fe^0 \rightarrow Fe^{2+} + 2e^- \text{ (Anodic reaction)} \quad (2)$$

$$2H_2O + O_2 + 4e^- \rightarrow 4OH^- \text{ (Cathodic reaction)} \quad (3)$$

$$2\ M + 4OH^- + :NR_n \rightarrow 2\ M:OH_2...NC_2 \rightarrow M + OH_2...NR_n \quad (4)$$

Table 1
The fitted electrochemical impedance data values obtained for the blank epoxy and the modified polymeric nanocomposites immersed in 3.5 wt% NaCl for different immersion times at room temperature.

Coatings	Time (day)	R_{po} (MΩ.cm²)	CPE_1 ($s^n\ \Omega^{-1}cm^{-2}$)	n_1	R_{ct} (MΩ.cm²)	CPE_2 ($s^n\ \Omega^{-1}\ cm^{-2}$)	n_2	R_s (Ohms)	W ($s^n\ \Omega^{-1}\ cm^{-2}$)	Goodness of fit
Scratched Blank epoxy	1	0.19	5.55×10^{-12}	0.83	0.18	7.69×10^{-12}	0.85	760.5	-	2.30×10^{-3}
	3	0.14	4.19×10^{-10}	0.80	0.13	3.23×10^{-10}	0.83	721.8	-	3.58×10^{-3}
	5	0.13	1.48×10^{-9}	0.76	0.09	2.69×10^{-9}	0.78	734.2	-	1.70×10^{-3}
	7	0.10	4.57×10^{-6}	0.65	0.03	1.54×10^{-6}	0.63	750.4	-	4.35×10^{-3}
Scratched epoxy-ZrO_2/IM	1	0.30	1.60×10^{-12}	0.86	0.42	5.24×10^{-9}	0.83	778.5	10.8	2.94×10^{-3}
	3	0.19	1.09×10^{-9}	0.84	0.31	5.34×10^{-6}	0.80	766.8	7.80	1.04×10^{-3}
	5	8.59	2.40×10^{-11}	0.90	1.12	2.33×10^{-9}	0.85	772.4	15.6	1.95×10^{-3}
	7	221.5	8.53×10^{-12}	0.94	555	1.899×10^{-12}	0.90	756.2	18.3	1.41×10^{-3}
Scratched epoxy-ZrO_2/PEI	1	0.37	3.43×10^{-12}	0.92	0.52	1.67×10^{-9}	0.90	749.7	11.3	5.23×10^{-3}
	3	0.22	1.49×10^{-10}	0.86	0.45	1.63×10^{-6}	0.84	734.6	10.66	2.05×10^{-3}
	5	7.34	3.86×10^{-12}	0.90	3.27	6.50×10^{-9}	0.86	726.3	16.2	1.55×10^{-3}
	7	1820	4.05×10^{-12}	0.94	2040	7.51×10^{-12}	0.92	724.2	17.8	1.65×10^{-3}
Scratched epoxy pre and top layer	1	1.07	3.82×10^{-9}	0.87	1.79	3.06×10^{-9}	0.88	731.2	10.72	1.77×10^{-3}
(epoxy-ZrO_2/IM) (epoxy-ZrO_2/PEI)	3	0.14	$1.72x\ 10^{-6}$	0.80	0.53	2.19×10^{-6}	0.85	735.7	8.64	1.64×10^{-3}
	5	9.2	1.59×10^{-12}	0.86	4.77	7.54×10^{-11}	0.90	745.4	13.84	1.60×10^{-3}
	7	2488	8.67×10^{-12}	0.90	3430	1.05×10^{-12}	0.92	750.2	15.88	1.68×10^{-3}

$$M + :NH_2 \rightarrow M:NH_2 \quad (5)$$

where M represents the metal steel (Fe). This adsorption behavior of the amine group from self-healing agent and inhibitor and complementing water replacement are the main contributing factor for protective behavior. The schematic showing the protective mechanism is demonstrated in Fig. 11.

10. Conclusion

The ZrO_2 nanoparticles were successfully modified with imidazole (IM) and polyethyleneimine (PEI) and added into the epoxy matrix at a fixed concentration of 1 wt%. To take the advantage of the synergistic effect of both corrosion inhibitor and self-healing agent, a double-layer (pre and topcoat) system was successfully developed. Various characterization techniques FTIR, TEM, EDX, TGA were done to confirm the successful modification of ZrO_2 nanoparticles with IM and PEI. UV–vis spectroscopy analysis validates the pH sensitivity and time dependence release of functional species from the ZrO_2 nanocarriers. The successful self-healing ability of the coatings was demonstrated by SEM. EIS analysis demonstrates that epoxy-based double-layer nanocomposite coatings exhibit superior corrosion protection (99.3%) characteristics compared to epoxy-ZrO_2/IM (91.9%) and epoxy-ZrO_2/PEI (97.2%) single layer coatinggs. The improved corrosion resistance of epoxy-based double-layer nanocomposite coatings can be ascribed to the synergistic effect of both corrosion inhibitor and self-healing agent present in distinct layers and their efficient release in response to the external stimuli (crack and pH change). The promising corrosion protection properties of epoxy-based double-layer nanocomposite coatings make them suitable for many industrial applications.

Funding: This research was funded by Qatar National Research Fund (a member of the Qatar Foundation), grant number NPRP Grant 11S–1226–170132. Statements made herein are solely the responsibility of the authors. Open Access funding provided by the Qatar National Library.

Declaration of Competing Interest

The authors declare that they have no known competing financial interests or personal relationships that could have appeared to influence the work reported in this paper.

Acknowledgment

The authors would like to thank the Central laboratory Unit (CLU), Qatar University, 2713, Doha, Qatar, for the SEM analysis facility. Open Access funding provided by the Qatar National Library.

Data availability

The raw/processed data required to reproduce these findings cannot be shared at this time due to legal or ethical reasons.

Appendix A. Supplementary data

Supplementary data to this article can be found online at https://doi.org/10.1016/j.matdes.2021.109839.

References

[1] M. Behzadnasab, S.M. Mirabedini, M. Esfandeh, Corrosion protection of steel by epoxy nanocomposite coatings containing various combinations of clay and nanoparticulate zirconia, Corros. Sci. 75 (2013) 134–141, https://doi.org/10.1016/j.corsci.2013.05.024.
[2] M.M. Popović, B.N. Grgur, V.B. Mišković-Stanković, Corrosion studies on electrochemically deposited PANI and PANI/epoxy coatings on mild steel in acid sulfate solution, Prog. Org. Coatings. 52 (2005) 359–365, https://doi.org/10.1016/j.porgcoat.2004.05.009.
[3] Y. González-García, S. González, R.M. Souto, Electrochemical and structural properties of a polyurethane coating on steel substrates for corrosion protection, Corros. Sci. 49 (2007) 3514–3526, https://doi.org/10.1016/j.corsci.2007.03.018.
[4] G.W. Walter, A critical review of the protection of metals by paints, Corros. Sci. 26 (1986) 27–38, https://doi.org/10.1016/0010-938X(86)90120-4.
[5] J. Wicks ZW, F.N. Jones, S.P. Peppas, Organic Coatings: Science and Technology Volume 1: Film Formation, Components and Appearance, Dry. Technol. 11 (1993) 1477.
[6] F. Hussain, M. Hojjati, M. Okamoto, R.E. Gorga, Review article: Polymer-matrix Nanocomposites, Processing, Manufacturing, and Application: An Overview, J. Compos. Mater. 40 (2006) 1511–1575, https://doi.org/10.1177/0021998306067321.
[7] M.F. Montemor, Hybrid nanocontainer-based smart self-healing composite coatings for the protection of metallic assets, in: Smart Compos. Coatings Membr., Elsevier Ltd, 2016: pp. 183–210. doi:10.1016/B978-1-78242-283-9.00007-5.
[8] P.A. Sørensen, S. Kiil, K. Dam-Johansen, C.E. Weinell, Anticorrosive coatings: A review, J. Coatings Technol. Res. 6 (2009) 135–176, https://doi.org/10.1007/s11998-008-9144-2.
[9] F. Ubaid, A.B. Radwan, N. Naeem, R.A. Shakoor, Z. Ahmad, M.F. Montemor, R. Kahraman, A.M. Abdullah, A. Soliman, Multifunctional self-healing polymeric nanocomposite coatings for corrosion inhibition of steel, Surf. Coatings Technol. 372 (2019) 121–133, https://doi.org/10.1016/j.surfcoat.2019.05.017.
[10] F. Ubaid, N. Naeem, R.A. Shakoor, R. Kahraman, S. Mansour, A. Zekri, Effect of concentration of DOC loaded TiO2 nanotubes on the corrosion behavior of smart coatings, Ceram. Int. 45 (2019) 10492–10500, https://doi.org/10.1016/J.CERAMINT.2019.02.111.
[11] M. Nawaz, N. Yusuf, S. Habib, R.A. Shakoor, F. Ubaid, Z. Ahmad, R. Kahraman, S. Mansour, W. Gao, M. Nawaz, N. Yusuf, S. Habib, R.A. Shakoor, F. Ubaid, Z. Ahmad, R. Kahraman, S. Mansour, W. Gao, Development and Properties of Polymeric Nanocomposite Coatings, Polymers (Basel). 11 (2019) 852, https://doi.org/10.3390/polym11050852.
[12] P. Vijayan P., M.A.S.A. Al-Maadeed, TiO2 nanotubes and mesoporous silica as containers in self-healing epoxy coatings, Sci. Rep. 6 (2016) 38812. doi:10.1038/srep38812.
[13] I.A. Kartsonakis, L.L. Danilidis, G.S. Pappas, G.C. Kordas, Encapsulation and release of corrosion inhibitors into titania nanocontainers, J. Nanosci. Nanotechnol. 10 (2010) 5912–5920, https://doi.org/10.1166/jnn.2010.2571.
[14] J.M. Falcón, F.F. Batista, I.V. Aoki, Encapsulation of dodecylamine corrosion inhibitor on silica nanoparticles, Electrochim. Acta 124 (2014) 109–118, https://doi.org/10.1016/j.electacta.2013.06.114.
[15] Y. Feng, Y.F. Cheng, An intelligent coating doped with inhibitor-encapsulated nanocontainers for corrosion protection of pipeline steel, Chem. Eng. J. 315 (2017) 537–551, https://doi.org/10.1016/j.cej.2017.01.064.
[16] S. Habib, E. Fayyad, M. Nawaz, A. Khan, R.A. Shakoor, Cerium Dioxide Nanoparticles as Smart Carriers for Self-Healing Coatings Cerium Dioxide Nanoparticles as Smart Carriers for Self-Healing Coatings (2020), https://doi.org/10.3390/nano10040791.
[17] Y. Lei, Z. Qiu, N. Tan, H. Du, D. Li, J. Liu, T. Liu, W. Zhang, X. Chang, Polyaniline/CeO2 nanocomposites as corrosion inhibitors for improving the corrosive performance of epoxy coating on carbon steel in 3.5% NaCl solution, Prog. Org. Coatings. 139 (2020), https://doi.org/10.1016/j.porgcoat.2019.105430 105430.
[18] I. Mohammadi, M. Izadi, T. Shahrabi, D. Fathi, A. Fateh, Enhanced epoxy coating based on cerium loaded Na-montmorillonite as active anti-corrosive nanoreservoirs for corrosion protection of mild steel: Synthesis, characterization, and electrochemical behavior, Prog. Org. Coatings. 131 (2019) 119–130, https://doi.org/10.1016/j.porgcoat.2019.02.016.
[19] M. Nawaz, R.A. Shakoor, R. Kahraman, M.F. Montemor, Cerium oxide loaded with gum Arabic as environmentally friendly anti-corrosion additive for protection of coated steel, Mater. Des. 198 (2020), https://doi.org/10.1016/j.matdes.2020.109361 109361.
[20] S. Habib, A. Khan, M. Nawaz, M.H. Sliem, R.A. Shakoor, R. Kahraman, A.M. Abdullah, A. Zekri, Self-healing performance of multifunctional polymeric smart coatings, Polymers (Basel). 11 (2019), https://doi.org/10.3390/polym11091519.
[21] A. Khan, A. Hassanein, S. Habib, M. Nawaz, R.A. Shakoor, R. Kahraman, Hybrid Halloysite Nanotubes as Smart Carriers for Corrosion Protection, ACS Appl. Mater. Interfaces 12 (2020) 37571–37584, https://doi.org/10.1021/acsami.0c08953.
[22] E. Shchukina, D. Grigoriev, T. Sviridova, D. Shchukin, Comparative study of the effect of halloysite nanocontainers on autonomic corrosion protection of polyepoxy coatings on steel by salt-spray tests, Prog. Org. Coatings. 108 (2017) 84–89, https://doi.org/10.1016/J.PORGCOAT.2017.03.018.
[23] E. Shchukina, D. Shchukin, D. Grigoriev, Halloysites and mesoporous silica as inhibitor nanocontainers for feedback active powder coatings, Prog. Org. Coatings. 123 (2018) 384–389, https://doi.org/10.1016/j.porgcoat.2015.12.013.
[24] Y. He, W. Xu, R. Tang, C. Zhang, Q. Yang, pH-Responsive nanovalves based on encapsulated halloysite for the controlled release of a corrosion inhibitor in epoxy coating, RSC Adv. 5 (2015) 90609–90620, https://doi.org/10.1039/C5RA19296J.

[25] Y. He, C. Zhang, F. Wu, Z. Xu, Fabrication study of a new anticorrosion coating based on supramolecular nanocontainer, Synth. Met. 212 (2016) 186–194, https://doi.org/10.1016/j.synthmet.2015.10.022.

[26] K.V. Yeole, I.P. Agarwal, S.T. Mhaske, The effect of carbon nanotubes loaded with 2-mercaptobenzothiazole in epoxy-based coatings, J. Coatings Technol. Res. 13 (2016) 31–40, https://doi.org/10.1007/s11998-015-9730-z.

[27] A. Bahrani, R. Naderi, M. Mahdavian, Chemical modification of talc with corrosion inhibitors to enhance the corrosion protective properties of epoxy-ester coating, Prog. Org. Coatings. 120 (2018) 110–122, https://doi.org/10.1016/j.porgcoat.2018.03.017.

[28] S. Habib, E. Fayyed, A. Shakoor, A. Kahraman, Ramazan Abdullah, Improved self-healing performance of polymeric nanocomposites reinforced with talc nanoparticles (TNPs) and urea-formaldehyde microcapsules (UFMCs), Arab. J. Chem. 14 (2020), https://doi.org/10.1016/j.arabjc.2020.102926 102926.

[29] M.F. Montemor, D.V. Snihirova, M.G. Taryba, S.V. Lamaka, I.A. Kartsonakis, A.C. Balaskas, G.C. Kordas, J. Tedim, A. Kuznetsova, M.L. Zheludkevich, M.G.S. Ferreira, Evaluation of self-healing ability in protective coatings modified with combinations of layered double hydroxides and cerium molibdate nanocontainers filled with corrosion inhibitors, Electrochim. Acta 60 (2012) 31–40, https://doi.org/10.1016/j.electacta.2011.10.078.

[30] D. Li, F. Wang, X. Yu, J. Wang, Q. Liu, P. Yang, Y. He, Y. Wang, M. Zhang, Anticorrosion organic coating with layered double hydroxide loaded with corrosion inhibitor of tungstate, Prog. Org. Coatings. 71 (2011) 302–309, https://doi.org/10.1016/j.porgcoat.2011.03.023.

[31] M. Serdechnova, S. Kallip, M.G.S. Ferreira, M.L. Zheludkevich, Active self-healing coating for galvanically coupled multi-material assemblies, Electrochem. Commun. 41 (2014) 51–54, https://doi.org/10.1016/j.elecom.2014.01.023.

[32] M. Behzadnasab, S.M. Mirabedini, K. Kabiri, S. Jamali, Corrosion performance of epoxy coatings containing silane treated ZrO2 nanoparticles on mild steel in 3.5% NaCl solution, Corros. Sci. 53 (2011) 89–98, https://doi.org/10.1016/j.corsci.2010.09.026.

[33] X. Lv, X. Li, N. Li, H. Zhang, Y. zhen Zheng, J. Wu, X. Tao, ZrO2 nanoparticle encapsulation of graphene microsheets for enhancing anticorrosion performance of epoxy coatings, Surf. Coatings Technol. 358 (2019) 443–451. doi:10.1016/j.surfcoat.2018.11.045.

[34] S.K. Dhoke, A.S. Khanna, T.J.M. Sinha, Effect of nano-ZnO particles on the corrosion behavior of alkyd-based waterborne coatings, Prog. Org. Coatings. 64 (2009) 371–382, https://doi.org/10.1016/j.porgcoat.2008.07.023.

[35] Y.-F. Zhu, L. Shi, J. Liang, D. Hui, K. Lau, Synthesis of zirconia nanoparticles on carbon nanotubes and their potential for enhancing the fracture toughness of alumina ceramics, Compos. Part B Eng. 39 (2008) 1136–1141, https://doi.org/10.1016/j.compositesb.2008.03.006.

[36] P.C. Okafor, X. Liu, Y.G. Zheng, Corrosion inhibition of mild steel by ethylamino imidazoline derivative in CO2-saturated solution, Corros. Sci. 51 (2009) 761–768, https://doi.org/10.1016/j.corsci.2009.01.017.

[37] S.M. Mirabedini, G.E. Thompson, S. Moradian, J.D. Scantlebury, Corrosion performance of powder coated aluminium using EIS, Prog. Org. Coatings. 46 (2003) 112–120, https://doi.org/10.1016/S0300-9440(02)00218-7.

[38] W.Q. Wang, C.K. Sha, D.Q. Sun, X.Y. Gu, Microstructural feature, thermal shock resistance and isothermal oxidation resistance of nanostructured zirconia coating, Mater. Sci. Eng., A 424 (2006) 1–5, https://doi.org/10.1016/j.msea.2005.10.025.

[39] A. Ershad-Langroudi, A. Rahimi, Effect of ceria and zirconia nanoparticles on corrosion protection and viscoelastic behavior of hybrid coatings, Iran. Polym. J. (English Ed. 23 (2014) 267–276, https://doi.org/10.1007/s13726-014-0222-2.

[40] J. Tedim, S.K. Poznyak, A. Kuznetsova, D. Raps, T. Hack, M.L. Zheludkevich, M.G. S. Ferreira, Enhancement of Active Corrosion Protection via Combination of Inhibitor-Loaded Nanocontainers, ACS Appl. Mater. Interfaces 2 (2010) 1528–1535, https://doi.org/10.1021/am100174t.

[41] W. Xu, Z. Wang, E.H. Han, S. Wang, Q. Liu, Corrosion performance of nano-ZrO2 modified coatings in hot mixed acid solutions, Materials (Basel). 11 (2018) 1–18, https://doi.org/10.3390/ma11060934.

[42] A. Chenan, S. Ramya, R.P. George, U. Kamachi Mudali, Hollow mesoporous zirconia nanocontainers for storing and controlled releasing of corrosion inhibitors, Ceram. Int. 40 (2014) 10457–10463, https://doi.org/10.1016/j.ceramint.2014.03.016.

[43] T. Ge, W. Zhao, X. Wu, Y. Wu, L. Shen, X. Ci, Y. He, Design alternate epoxy-reduced graphene oxide/epoxy-zinc multilayer coatings for achieving long-term corrosion resistance for Cu, Mater. Des. 186 (2020), https://doi.org/10.1016/j.matdes.2019.108299 108299.

[44] E. Salahinejad, M.J. Hadianfard, D.D. Macdonald, M. Mozafari, D. Vashaee, L. Tayebi, A new double-layer sol–gel coating to improve the corrosion resistance of a medical-grade stainless steel in a simulated body fluid, Mater. Lett. 97 (2013) 162–165, https://doi.org/10.1016/j.matlet.2013.01.111.

[45] H. Kim, A.L. Yarin, M.W. Lee, Self-healing corrosion protection film for marine environment, Compos. Part B Eng. 182 (2020), https://doi.org/10.1016/j.compositesb.2019.107598 107598.

[46] R. Ramasamy, Vibrational Spectroscopic Studies of Imidazole, Armen. J. Phys. 8 (2015) 51–55.

[47] S. Lakard, G. Herlem, B. Lakard, B. Fahys, Theoretical study of the vibrational spectra of polyethylenimine and polypropylenimine, J. Mol. Struct. (Thoechem) 685 (2004) 83–87, https://doi.org/10.1016/j.theochem.2004.06.042.

[48] D.R. Uhlmann, B.J.J. Zelinski, G.E. Wnek, The Ceramist as Chemist - Opportunities for New Materials, MRS Proc. 32 (1984) 59, https://doi.org/10.1557/PROC-32-59.

[49] S.K. Saha, P. Pramanik, Aqueous sol-gel synthesis of powders in the ZrO2 SiO2 system using zirconium formate and tetraethoxysilane, J. Non. Cryst. Solids. 159 (1993) 31–37, https://doi.org/10.1016/0022-3093(93)91279-C.

[50] S.W. Lee, R.A. Condrate Sr., The infrared and Raman spectra of ZrO2-SiO2 glasses prepared by a sol-gel process, J. Mater. Sci. 23 (1988) 2951–2959, https://doi.org/10.1007/BF00547474.

[51] S. Jayakumar, P.V. Ananthapadmanabhan, K. Perumal, T.K. Thiyagarajan, S.C. Mishra, L.T. Su, A.I.Y. Tok, J. Guo, Characterization of nano-crystalline ZrO2 synthesized via reactive plasma processing, Mater. Sci. Eng. B Solid-State Mater. Adv. Technol. 176 (2011) 894–899, https://doi.org/10.1016/j.mseb.2011.05.013.

[52] M. Manyangadze, N.H.M. Chikuruwo, T.B. Narsaiah, C.S. Chakra, M. Radhakumari, G. Danha, Enhancing adsorption capacity of nano-adsorbents via surface modification: A review, South African J. Chem. Eng. 31 (2020) 25–32, https://doi.org/10.1016/j.sajce.2019.11.003.

[53] M. Abdallah, H.E. Megahed, M. Sobhi, Ni2+ cation and imidazole as corrosion inhibitors for carbon steel in sulfuric acid solutions, Monatsh. Chem. 141 (2010) 1287–1295, https://doi.org/10.1007/s00706-010-0396-z.

[54] J. Aljourani, K. Raeissi, M.A. Golozar, Benzimidazole and its derivatives as corrosion inhibitors for mild steel in 1M HCl solution, Corros. Sci. 51 (2009) 1836–1843.

[55] M. Nawaz, S. Habib, A. Khan, R.A. Shakoor, R. Kahraman, Cellulose microfibers (CMFs) as a smart carrier for autonomous self-healing in epoxy coatings, New J. Chem. (2020), https://doi.org/10.1039/C9NJ06436B.

[56] K.A. Curtis, D. Miller, P. Millard, S. Basu, F. Horkay, P.L. Chandran, Unusual salt and pH induced changes in polyethylenimine solutions, PLoS ONE 11 (2016) 1–20, https://doi.org/10.1371/journal.pone.0158147.

[57] F. Jiang, W. Zhao, Y. Wu, Y. Wu, G. Liu, J. Dong, K. Zhou, A polyethyleneimine-grafted graphene oxide hybrid nanomaterial: Synthesis and anti-corrosion applications, Appl. Surf. Sci. 479 (2019) 963–973, https://doi.org/10.1016/j.apsusc.2019.02.193.

[58] R. Fuchs-Godec, M.G. Pavlović, Synergistic effect between non-ionic surfactant and halide ions in the forms of inorganic or organic salts for the corrosion inhibition of stainless-steel X4Cr13 in sulphuric acid, Corros. Sci. 58 (2012) 192–201, https://doi.org/10.1016/j.corsci.2012.01.027.

[59] C.H. Hsu, F. Mansfeld, Technical Note: Concerning the Conversion of the Constant Phase Element Parameter Y0 into a Capacitance, CORROSION. 57 (2001) 747–748, https://doi.org/10.5006/1.3280607.

[60] M. Ganjaee Sari, B. Ramezanzadeh, M. Shahbazi, A.S. Pakdel, Influence of nanoclay particles modification by polyester-amide hyperbranched polymer on the corrosion protective performance of the epoxy nanocomposite, Corros. Sci. 92 (2015) 162–172, https://doi.org/10.1016/j.corsci.2014.11.047.

[61] T.A. Söylev, M.G. Richardson, Corrosion inhibitors for steel in concrete: State-of-the-art report, Constr. Build. Mater. 22 (2008) 609–622, https://doi.org/10.1016/j.conbuildmat.2006.10.013.

[62] F. Wombacher, U. Maeder, B. Marazzani, Aminoalcohol based mixed corrosion inhibitors, Cem. Concr. Compos. 26 (2004) 209–216, https://doi.org/10.1016/S0958-9465(03)00040-4.

[63] X. He, Y. Jiang, C. Li, W. Wang, B. Hou, L. Wu, Inhibition properties and adsorption behavior of imidazole and 2-phenyl-2-imidazoline on AA5052 in 1.0M HCl solution, Corros. Sci. 83 (2014) 124–136, https://doi.org/10.1016/j.corsci.2014.02.004.

[64] H.S. Ryu, J.K. Singh, H.S. Lee, W.J. Park, An Electrochemical Study to Evaluate the Effect of Calcium Nitrite Inhibitor to Mitigate the Corrosion of Reinforcement in Sodium Chloride Contaminated Ca(OH)2 Solution, Adv. Mater. Sci. Eng. 2017 (2017), https://doi.org/10.1155/2017/6265184.